Published in final edited form as:

Brain Stimul. 2021 ; 14(2): 261–272. doi:10.1016/j.brs.2021.01.006.

Bidirectional and state-dependent modulation of brain activity by transcranial focused ultrasound in non-human primates

Pai-Feng Yang[a,b], **M. Phipps Anthony**[a], **Sumeeth Jonathan**[a], **Allen T. Newton**[a,b], **Nellie Byun**[a], **John C. Gore**[a,b,c], **William A. Grissom**[a,c], **Charles F. Caskey**[a,b,1], **Li Min Chen**[a,b,*,1]

[a]Vanderbilt University Institute of Imaging Science, Vanderbilt University, Nashville, TN, USA

[b]Department of Radiology and Radiological Sciences, Vanderbilt University Medical Center, Nashville, TN, USA

[c]Department of Biomedical Engineering, Vanderbilt University, Nashville, TN, USA

Abstract

Transcranial focused ultrasound (FUS) stimulation under MRI guidance, coupled with functional MRI (fMRI) monitoring of effects, offers a precise, noninvasive technology to dissect functional brain circuits and to modulate altered brain functional networks in neurological and psychiatric disorders. Here we show that ultrasound at moderate intensities modulated neural activity bi-directionally. Concurrent sonication of somatosensory areas 3a/3b with 250 kHz FUS suppressed the fMRI signals produced there by peripheral tactile stimulation, while at the same time eliciting fMRI activation at inter-connected, off-target brain regions. Direct FUS stimulation of the cortex resulted in different degrees of BOLD signal changes across all five off-target regions, indicating that its modulatory effects on active and resting neurons differed. This is the first demonstration of the dual suppressive and excitative modulations of FUS on a specific functional circuit and of ability of concurrent FUS and MRI to evaluate causal interactions between functional circuits with neuron-class selectivity.

Keywords

Transcranial focused ultrasound; Primates; fMRI; Neuromodulation; Brain circuit; Hand; Somatosensory

*Corresponding author. Department of Radiology and Radiological Sciences, Institute of Imaging Science, Vanderbilt University Medical Center, AA 1105 MCN, 1161 21st Ave. S., Nashville, TN, 37232, USA. limin.chen@vanderbilt.edu (L.M. Chen).

Author contributions

LMC, CC, WAG and JCG designed the experiment. PFY, MAP, SJ, AN, NB, WAG, CC, and LMC participated data collection. PFY and LMC prepared. MAP, SJ and LMC prepared. LMC & PFY wrote the first draft of the manuscript and revised the manuscript together with CC, WAG and JCG. PFY, SJ and MAP contributed to the writing of the main manuscript text.

[1]These authors are equally responsible for the project.

Declaration of competing interest

The authors declare no competing interests.

Appendix A. Supplementary data

Supplementary data to this article can be found online at https://doi.org/10.1016/j.brs.2021.01.006.

Introduction

Regions and circuits within a healthy brain interact in a coordinated fashion to maintain and execute various functions, while dysfunction in specific networks underlie many psychiatric and neurological disorders [1–7]. Targeted neuromodulation of a particular brain region by transcranial focused ultrasound stimulation (tFUS) has emerged as a powerful tool for evaluating functional connections and causal interactions between regions and allowing investigations of the contributions of individual brain regions to specific operations and functions in both healthy and disease conditions. It is also a potential therapeutic intervention for modulating network activities in neurological and psychiatric disorders. Like other widely used neural stimulation methods such as transcranial electrical stimulation (TES) [8–11], intracranial electrical stimulation (ICS) [12–15], deep brain stimulation (DBS) [16–18], and transcranial magnetic stimulation (TMS) [4,19–22], tFUS has gained wide-recognition as a next generation neuromodulation technology. Among these other methods, only TES and TMS are noninvasive, but they can localize primarily only superficial brain structures with centimeter-scale precision, while the rest are highly invasive, requiring surgical placement of electrodes into the brain. More importantly, some of these methods are unable to use image guidance or offer real-time functional monitoring that are essential features for evaluating the effects and consequences of neuromodulation. In this context, MRI guided transcranial FUS potentially offers a superior alternative noninvasive neuromodulation technology with several essential characteristics: (1) millimeter scale spatial localization under MRI guidance; (2) access to all parts of the brain; and (3) integrated functional monitoring when combined with simultaneous functional magnetic resonance imaging (fMRI) of brain activity. Real-time image guidance itself improves the spatial precision of FUS targeting while functional MRI monitoring reports FUS's action in both local (targeted) and other affected (off-target, downstream) brain regions.

Using BOLD (blood oxygenation level dependent) fMRI as a functional readout, we previously demonstrated that 250 kHz US pulses at 935 kPa free-field amplitude can excite local neurons in targeted somatosensory areas 3a/3b as well as downstream, interconnected neurons in off-target brain regions [23]. Theoretically, FUS can modulate neural activity in both positive (excitation) and negative (inhibitory) directions via actions on different ionic channels on neuron members for example [24]50]. This dual capacity is a highly desirable feature for a therapeutic technique. Moreover, the possibility of state-dependent modulatory effects of FUS, such as those reported in TMS literature [25,26], can also have significant implications for future FUS applications on modulating brain activity in different brain cognitive states or in physiology versus pathological states. Previous FUS studies have used varying parameters in different experimental models and reported both excitation and suppression effects on the target, but the precise mechanisms of action of FUS on neurons remains elusive. The ability to simultaneously monitor FUS's action at both target and off-target regions offers an effective way to examine the neural basis of FUS's effects because activity of only excitatory neurons can propagate and lead to detectable BOLD activation at down-stream off-target brain regions [23]. Figs. 1–6.

The current study focused on exploring possible inhibitory effects of FUS at medium-amplitudes (med-FUS, 425 kPa free-field at 250 kHz) and their influence on neuron populations and functional circuits using fMRI of the sensorimotor system of the macaque brain as a model system. Previous studies indicate that the complexity of brain circuits may play a key role in the efficacy of neuromodulation. In this respect, the macaque brain is advantageous because of its close resemblance in structure and function to the human brain. Macaque monkeys have been well characterized by fMRI and intracranial electrophysiology as well as by invasive and post-mortem studies [27,28]. We have developed robust fMRI paradigms that allow us to reliably map touch responses in the brains of non-human primates [29–34], and have demonstrated the ability to detect high-amplitude FUS-induced neuromodulation effects [23], in which the used FUS was twice as high in amplitude. we refer to the current parameters as “med-FUS” to indicate medium amplitude. Here we report that med-FUS modulated activity of neurons at the target in dual directions (excitation and suppression) and in a state-dependent manner. We propose that this simultaneous excitatory and suppressive neuromodulation is mediated by activation of large excitatory pyramidal and small inhibitory interneurons, respectively. The potential for neuron-selective modulation by FUS is highly significant for potential clinical translation. Figs. 7 and 8.

Material and methods

Animal preparation

Two adult female macaque monkeys (*M. fascicularis*) were underwent six MRI experiments (three for each monkey). A total of 50 fMRI scans (runs) were collected. Animals were initially sedated with ketamine hydrochloride (10 mg/kg) and atropine sulfate (0.05 mg/kg) and then anesthetized with isoflurane (1.0%-1.5%) delivered in oxygen. After intubation, each animal was placed in a custom-designed MR stereotaxic frame with the head secured by ear bars, eye, and mouthpieces. During functional MRI data acquisition, animals were maintained at a light (0.85–1.0% isoflurane) and stable level of anesthesia. A solution of 2.5% dextrose in saline solution was infused intravenously (3 ml/kg/h) to prevent dehydration. Animals were artificially ventilated throughout the experiment. Temperature was maintained by means of a circulating water blanket. Heart rate and peripheral capillary oxygen saturation (SpO2; Nonin), respiration pattern and end-tidal CO_2 (24–32 mmHg; SurgiVet) were continuously monitored and maintained during the entire procedure. All procedures were conducted in accordance with National Institutes of Health guidelines and were approved by the Institutional Animal Care and Use Committee of Vanderbilt University.

Peripheral tactile stimulation protocol

The fingers were stabilized with modeling clay, palm side up, leaving the glabrous skin of the distal finger pads available for stimulation. Innocuous tactile stimuli were delivered at 8 Hz on the distal finger pads of D2 and D3 of the left hand in 0.44 mm vertical displacements via two rounded probes 2 mm in diameter driven by an S88 Grass stimulator. For each fMRI tactile stimulation run, 30-s duration blocks of tactile stimuli were repeated seven times with 30 s baseline periods interleaved. The probes were in contact with the skin on the digits during baseline periods.

FUS parameters and presentation paradigm

During fMRI data acquisition, FUS pulses were delivered in a block-based scheme identical to the tactile stimuli in seven 30 s FUS on/off cycles (Fig. 1). During an “on” block, a 250 kHz, 300 ms pulse was emitted at 0.333 Hz from a spherically focused MR-compatible transducer (H115 diameter = 64 mm ROC = 63.2 mm, Sonic Concepts, Bothell, WA) coupled via a custom water cone filled with 80% D_2O that had been at undisturbed for 24 h to allow large bubbles to float out of solution. The D_2O was used to replace most of the H2O to reduce signal intensities and geometric distortions of MR images due to ineffective shimming. A single 300 ms pulse consisted of 63-cycle bursts repeated at 2 kHz (50% duty cycle–see Fig. 1 for FUS pulse design). The FUS transducer was driven by an arbitrary waveform generator (Agilent 33511B, Santa Clara, CA, USA) connected to an RF power amplifier (E&I A150, Rochester, NY, USA). The free field peak negative pressure at the spatial focus during this pulse was 425 kPa, which is about 45% of the 935 kPa pulses used in our previous study [23]. The free field spatial peak temporal average intensity (Ispta) was 27.1 mW/cm^2 and the free field spatial peak pulse average intensity (I_{sppa}) was 6.0 W/cm^2. At 250 kHz we estimate 58% transmission through a macaque skull yielding a PNP of 247 kPa, an Ispta of 9.1 mW/cm^2, and an I_{sppa} of 2.0 W/cm^2. A custom microcontroller program coordinated pulsing for tactile, FUS, and tactile + FUS stimulation. The procedure resulted in 10 FUS bursts per “on” block. The maximum free field pressure of the transducer was measured by placing a calibrated needle (for spatial peak pressures at which the MI was less than 1.4, H-0400 Onda Corp.) or fiber optic hydrophone (at higher pressures, FOH, Precision Acoustics, Dorchester, UK) at the focus of the transducer and recording the peak negative pressure at different input amplitudes.

Use of optical tracking and MRI-ARFI beam mapping methods to localize ultrasound beam on target

Delivering US modulation at the target with high precision is critical for our studies. We used optical tracking for stereotactic neuronavigation and to target the FUS beam to the area 3a/3b tactile region that was pre-defined by fMRI (Fig. 2A and B). Then, before fMRI scanning, we confirmed the location and actual delivery of FUS with transcranial MR-acoustic radiation force imaging (MR-ARFI) (Fig. 2C and D), which measures the transient tissue displacements induced by a short FUS pulse [35] as described below. The FUS transducer was first positioned over the region posterior to the central sulcus, where the area 3a/3b of the primary somatosensory cortex (S1) resides, on the right hemisphere ipsilateral to the tactile stimulation side of the left hand. Transmission gel was placed over the scalp to ensure adequate acoustic coupling. Five 15 mm MRI-visible fiducial markers (MM3002, IZI Medical Products, Owings Mills, MD) were placed on the stereotactic frame (one on each eye bar and three on the two ear bars) to enable optical tracking outside the MRI scanner. Briefly, the location and trajectory of the free-field FUS beam were estimated by tracking the position of the transducer (NDI Polaris, Ontario, Canada) and registering its position in physical space to the imaging space relative to the fixed positions of fiducials. Details of our optical tracking-based FUS targeting method followed our prior work [36]. Our average targeting registration error with this method was estimated to be less than 3 mm.

Prior to applying FUS, knowledge of the location of the acoustic focus must be obtained to verify that the ultrasound beam is reaching the target. We used an optically tracked MR-ARFI pulse sequence optimized for this FUS transducer to monitor the tissue displacements (proportional to acoustic intensity) induced by a short FUS pulse to map the ultrasound beam *in situ*. Displacement images were acquired using a 2D single-slice spin-echo MRI acquisition (12.0 × 12.0 cm^2 FOV; 60 × 60 matrix; 2.0 × 2.0 mm^2 voxel size; 1 slice; 4.0 mm slice thickness; TE/TR 17/1000 ms) with unipolar motion-encoding gradients (3 ms duration; 40 $mT•m^{-1}$ strength) to generate ARFI contrast. The motion-encoding gradients were oriented parallel to the ultrasound beam and the imaged slice was prescribed at the optically tracked location of the acoustic focus. Sonications were performed at 802 kHz for 4.5 ms (3609 cycles) with a maximum free-field pressure of 2.81 MPa and a duty cycle of 0.23%. Displacement images were reconstructed using complex phase subtraction of four phase images with switched polarity motion-encoding gradients and with or without sonications, which were acquired in an interleaved fashion, for a total scan time of 4.0 min to produce one displacement image. Images were reconstructed offline in MATLAB 2017a (MathWorks, Natick, MA). Our MR-ARFI beam mapping method was non-invasive and followed our and others prior work [35,37].

By determining the transducer location during optical tracking, the projected free-field ultrasound beam and the subsequently acquired displacement image could be overlaid on high-resolution T2*-weighted structural images in the targeted brain region where BOLD activation foci were encoded (Fig. 2E and F). Detailed equations describing the coordinate transforms relating these image volumes (optically tracked FUS beam, MR-ARFI displacement image, and T2*-weighted structural brain volume) are derived in our prior work [36].

MRI data acquisition

All MRI scans were performed on a 7T Philips Achieva magnet with a customized surface transmit-receive coil (inner diameter = 6 cm) centered over the primary (S1) and secondary (S2) somatosensory cortices of the right hemisphere. Three types of MR images were acquired. 3D T1-weighted high-resolution isotropic volume (THRIVE) images to localize the fiducial markers placed around the US probe for aligning and localizing the US beam to structural MR images (TE = 1.89 ms, TR = 4 ms, 400 × 400 x 140 matrix, 0.35 × 0.35 2 mm^3 voxel size, flip angle 10°, NSA = 1). A series of nine T2*-weighted multi-slice gradient echo high-resolution structural coronal images (TE = 27 ms, TR = 500 ms, 768 × 768 x 9 matrix, 0.104 × 0.104 1 mm^3 voxel size) were also collected. FMRI data were acquired from the same slices using a single-shot gradient echo planar imaging (GE-EPI) sequence (TE = 16 ms, TR = 2 s, 0.625 × 0.625 1 mm^3 voxel size, 128 × 128 × 9 matrix, interleaved slices, linear K space filling). An extra navigator echo was collected with no phase encoding prior to the acquisition of the actual image data. This echo is used to correct for phase variations typically caused by motion. FMRI data with tactile stimulation of distal digits and/or FUS were collected with the same fMRI acquisition parameters. To maximize activation detection, we presented two (tactile alone, tactile + FUS) or three experimental conditions (tactile alone, tactile + med-FUS, med-FUS alone) in an interleaved manner during each fMRI data acquisition run. In a typical interleaved session, a total of 4–6 runs

were acquired (435 vol per two-condition run and 635 vol per three-condition run). The anesthesia level was closely monitored and adjusted, so that vital signals remained very stable (heart rate:160 ± 3; end tidal CO_2: 34 ± 1, and oxygen saturation, spO_2: 99 ± 1%). A total of 51 runs from six imaging sessions (three sessions from each monkey) were included in the fMRI time course analysis.

FMRI data analysis

Pre-processing: FMRI signals, acquired during stimulation (tactile, FUS, tactile + FUS), went through standard pre-processing steps of slice timing (3dTshift, AFNI) and 3-D motion correction (3dvolreg, AFNI), and were then spatially smoothed using an isotropic Gaussian filter kernel with a full width at half maximum of 1 mm (3dmerge, AFNI). Functional EPI images were up-sampled from 0.625 × 0.625 × 1 mm^3 to 0.312 × 0.312 × 1 mm^3, and coregistered with corresponding T2*-weighted high-resolution anatomical images using a linear image registration tool (3dAlli-neate, AFNI) for display. The fMRI EPI data were temporally smoothed with a low-pass filter with cutoff frequency of 0.25 Hz (fslmaths, FSL).

FMRI activation maps: FMRI activation maps were created using a cross-correlation function between the signal time courses of each voxel and the boxcar predictor of the Hemodynamic Response Function (HRF) convolved stimulus presentation paradigm (3dDe-convolve, AFNI). Activation was defined as voxels that exhibited significantly correlated BOLD signal changes that were organized in a minimum of five up-sampled continuous voxels (cluster size of 0.49 mm^3). All fMRI activation maps (tactile alone, tactile + FUS, or FUS alone) were thresholded with a statistical t-value of 3.3 (p = 0.001, FDR corrected), spatially interpolated and then superimposed on the corresponding high-resolution T2*-weighted anatomical images. For localizing activation and identifying voxels for BOLD fMRI time courses analysis, two types of fMRI activation maps were generated, single condition and subtraction maps. Single condition activation maps allow us to detect and localize the strongest response voxel to a particular stimulation condition (i.e., tactile or FUS). Subtraction maps (difference maps between two experimental conditions) allows us to separate voxels that exhibit preferential responses to one condition over another, such as tactile alone versus tactile + FUS. Subtracting two different condition maps maximizes the identification of voxels that were strongly influenced by the addition of FUS during tactile stimulation (Fig. 3D). We also generated activation overlap maps to illustrate the spatial relationships of different activation foci (Fig. 4).

Quantification of time course of BOLD signal

Regions of interest (ROI)-based time course analyses were performed. We focused the time course analysis on the target and five off-target regions that are known to be part of the touch circuit and have shown consistent fMRI activations across scans and animals. Voxels that exhibited signal changes at t = 3.3, which is p = 0.001 with FDR = 0.05 correction, was used as a threshold to define activated voxels and included in the time course quantification. Three types of voxels were defined: (1) voxels activated by a single experimental condition: tactile or FUS stimulation; (2) voxels that showed significant differences in fMRI signal amplitude between two experimental conditions: tactile versus tactile + FUS; and (3) white

matter voxels. We extracted BOLD signal time courses from activated voxels within each anatomically defined ROI (using a macaque monkey brain atlas [38]) to quantify the amplitudes and temporal profiles of the BOLD signal changes to stimulation. WM voxels were defined based on anatomical MR images. We calculated the time course of the percent signal change by subtracting the mean baseline signal prior to stimulus onset from the mean BOLD signals of three peak volumes during the stimulation period, and then dividing it by the baseline signal (peak-baseline)/baseline %. Baseline signal was calculated by averaging the signal amplitude of three image volumes before the stimulus onset. BOLD peak amplitudes were calculated in each stimulus block from the 12 plateau image volumes during stimulus presentation. Measures were averaged across runs, scan sessions, and animals, and were examined for statistical significance using one-way ANOVA followed by Tukey's test between tactile, tactile + FUS, and FUS alone stimulation conditions. A $p < 0.05$ was considered statistically significant. ROI-based BOLD time course plots are presented as the mean ± standard error of the mean (SEM).

Results

FMRI visualization of touch circuits and beyond

We first mapped tactile circuits in the macaque brain using an 8 Hz vibrotactile stimulation of the distal digits to localize target regions in primary somatosensory area 3a/3b, in each animal. 8 Hz stimulation of the hand activates low threshold mechanoreceptors in the skin and elicits vibrotactile sensation in awake humans. The group of brain regions engaged in processing such stimuli are reliably activated by fMRI. Fig. 3 illustrates the touch and associated network detected by BOLD fMRI during vibrotactile stimulation of two distal finger pads simultaneously of macaque monkeys at 7T under light anesthesia. Consistent with previous observations in humans and non-human primates [29,30,39–41], BOLD activation was detected in the ventroposterior lateral (VPL) nucleus of the thalamus, the primary (areas 3a/3b and areas 1/2 of S1) and secondary (S2) somatosensory cortices, as well as in associated brain regions, including posterior insular (Ins) and midcingulate (MCC) cortices (Fig. 3A). These tactile stimulus-evoked BOLD activation patterns were observed repeatedly across imaging sessions and animals, and were used as functional readouts to determine the effects of FUS at the target and off-target brain regions.

FUS stimulation suppressed tactile stimulus-evoked fMRI responses at the target and off-target regions

We next tested the hypothesis that 250 kHz med-amplitude FUS (med-FUS) pulses cause inhibitory effects on targeted tactile neurons. We chose the functionally defined touch region in areas 3a/3b as the target because it is the first cortical relay station within touch circuits, and direct inhibition of this region would likely lead to a general reduction of tactile responses in off-target regions within the same circuit. We used our optical tracking method to place the FUS beam at the area 3a/3b functionally defined by fMRI, and then concurrently insonated the target during tactile stimulation applied in 30 s on/off cycles. Compared to the tactile stimulation-evoked fMRI activation maps, the addition of FUS pulses drastically reduced tactile-evoked activation at the target and in associated networks (off-target regions).

When the same threshold was used for displaying fMRI activation maps, fewer brain regions showed detectable BOLD activation to identical tactile stimulations (compare Fig. 3B–A).

To identify those brain regions in which BOLD signals were most affected by FUS, we generated difference images by calculating beta values and their standard deviations for the three experimental conditions of medium amplitude FUS alone, tactile stimulation with med-FUS, and without med-FUS (tactile alone). The blue patches in Fig. 3D show the brain regions (voxels) that exhibited the greatest BOLD signal differences between the two experimental conditions compared. Reduced tactile responses were detected at the target (areas 3a/3b) and many off-target regions. At the target, the voxels that showed fMRI responses to both conditions (tactile versus tactile + med-FUS) mainly overlapped. At the off-target regions, such as thalamus and S2 cortex, however, the tactile + med-FUS condition as well as med-FUS alone elicited additional, spatially segregated areas of activation in zones that were outside the original tactile circuit (see green outlines in Fig. 4A). These observations indicate that med-FUS not only suppressed the tactile-evoked response at the targeted areas 3a/3b, but also elicited neural activation in inter-connected non-tactile zones. Schematic illustration of the peak locations of each activation focus in each experimental condition highlights their spatial segregation in some areas (different color dots in Fig. 5).

Differential BOLD responses to tactile, med-FUS and tactile + med-FUS stimulations at the target and a subset of off-target brain regions

We next examined the fMRI signal differences in different experimental conditions (tactile alone, med-FUS alone, and tactile + med-FUS) by extracting BOLD signals from those voxels that exhibited the most significant (largest t-value) changes in the target and off-target regions. Using tactile stimulation alone as a natural functional control, the comparisons allow us to determine how mFUS interacts with cortex (the target area 3b/3a) at resting state (med-FUS alone with no tactile stimulation) and when the neurons are activated by tactile stimulation (med-FUS + tactile). Fig. 6 shows fMRI signal differences between three experimental conditions in the target and five off-target regions. Two features stand out in the time course plots. First, addition of med-FUS during tactile stimulation significantly reduced tactile stimulation evoked BOLD signal increases at the target (area 3a/3b) (tactile: 0.34 ± 0.03 (mean ± standard error); med-FUS + tactile: 0.28 ± 0.03, $p < 0.05$, one-way ANOVA followed by Tukey's test) and each of the five off-target ROIs (compare the red and blue columns in Fig. 6H) (tactile: 0.26 ± 0.03, 0.35 ± 0.03, 0.25 ± 0.04, 0.03 ± 0.04, 0.21 ± 0.04, 0.02 ± 0.005; med-FUS + tactile: 0.19 ± 0.03, 0.25 ± 0.04, 0.12 ± 0.03, 0.17 ± 0.03, 0.01 ± 0.005; for area 1/2, S2, Insula, MCC, VPL, WM, respectively). Second, compared to tactile-evoked responses, med-FUS alone induced BOLD signal changes that varied across ROIs (compare the orange with red columns in Fig. 6H). At the target area 3a/3b, BOLD signal changes evoked by tactile + med-FUS (0.28 ± 0.03) and med-FUS alone (0.21 ± 0.04) did not differ but were significantly weaker ($p < 0.05$, one-way ANOVA followed by Tukey's test) than those evoked by tactile stimulation alone (see the blue and orange column groups in Fig. 6H). Similar signal differences were present in off-target S2 (tactile + med-FUS, 0.25 + 0.04; med-FUS, 0.25 ± 0.04). In contrast, in the off-target areas 1/2 and insular cortices, the magnitudes of med-FUS elicited signal changes were comparable to those for tactile stimulation (compare the first and third column groups in Fig. 6H) but were

significantly stronger than the tactile + med-FUS condition (see values in the table in supplementary information). In the thalamic VPL nucleus, there were no significant differences in the response magnitudes in all three conditions. In the MCC, med-FUS elicited the weakest BOLD signal changes (0.07 ± 0.04) compared to tactile alone (0.3 ± 0.04) or tactile + med-FUS (0.17 ± 0.03). In the control white matter region, the BOLD signal changes were negligible (the last column group in Fig. 6H). In summary, the relative fMRI signal amplitudes in three different stimulation conditions differed across off-target regions. This observation indicates that med-FUS's modulations of fMRI signals are likely mediated via neural activity changes. We also observed significantly faster BOLD responses in S2 (Fig. 6I) (med-FUS + tactile, 5.75 ± 0.19 ms; tactile: 6.03 ± 0.19 ms). This observation suggests that med-FUS likely interacted differently with areas 3a/3b cortical neurons during different brain states and resulted in dual modulatory outcomes: suppressing (likely via small inhibitory interneurons) of activity of tactile neurons elicited by peripheral tactile stimulation and directly exciting area 3a/3b neurons (likely via excitatory pyramidal neurons) that lead to the activation of interconnected downstream neurons in other off-target brain regions. The mean values along with their standard errors are presented in supplementary Tables S1 and S2.

To understand how FUS modulates influence at off-target regions, we plotted the signal differences between target and off-target regions for each experimental condition by normalizing signals to that of target (Fig. 7B) and the relative signal changes induced by FUS (with and without tactile stimulation) by normalizing signals to those of evoked by tactile stimulation (Fig. 7A). We found that concurrent presentation of med-FUS suppressed tactile-evoked BOLD signal changes (shown as negative signal changes) at the target (area 3a/3b) as well as in all of the off-target regions of area 1/2, S2, insula, MCC, and VPL of thalamus (Fig. 7A). Med-FUS stimulation alone, however, evoked BOLD signal changes that were weaker than those to tactile stimulation at the target region of area 3a/3b and at five off-target regions (compare blue and orange bars in Fig. 7A. Med-FUS elicited stronger than tactile responses in area 1/2. When we normalize the BOLD signal changes to that of the target area 3a/3b, concurrent delivery of med-FUS with tactile stimuli suppressed the tactile-evoked activations in the five off-target regions, but to different degrees (compare orange to blue curves in Fig. 7B). The greatest suppression was observed in the insular cortex. Med-FUS alone, however, elicited stronger BOLD activation in area 1/2 and insular cortices, but weaker activation in MCC, when normalized to tactile activation of area 3a/3b (compare orange with blue curves in Fig. 7B). There was no difference detected between conditions in S2. The BOLD signal changes in different conditions are summarized in Fig. 7C and D. Together, the BOLD signal time course results support the state-dependent dual modulatory actions of med-FUS. The inter-regional differences in response magnitudes and latencies indicate that med-FUS likely exerts its modulation simultaneously on different types of neurons, which in turn affected distinct groups of neurons in off-target regions that likely belong to different functional circuits. The differential off-target effects on different brain regions imply that the underlying neuronal and circuit actions of med-FUS could be associated with their specific functional connections to the target area 3a/3b.

Proposed dual neuromodulation model of medium amplitude FUS

Based on the findings in our previous report [23] and those presented here, we propose a state-dependent dual neuromodulatory model of medium amplitude (med-FUS) on two types of neurons: small local inhibitory interneurons at the cortical activation state and communicative pyramidal neurons (Fig. 8) at resting state. Neurons excited by med-FUS in area 3a/3b likely connect to different groups of neurons in different functional circuits, which do not belong to the typical low-threshold tactile neurons that can be driven by 8 Hz vibrotactile stimulation of peripheral skin. The distinct activation pattern induced by concurrent tactile and med-FUS could reflect the net modulatory outcomes via specific functional connections between the stimulated target and off-target brain regions.

Discussion

The ability to modulate brain activity with high spatial precision is highly significant and potentially may have translational clinical applications in both diagnosis and therapy. Transcranial FUS has been proven repeatedly to be an effective neuromodulation tool for humans and animals, and can alter subjective sensation, animal behavior, neuronal electrical activity, and BOLD signal changes [42,43]. There have been prior reports of both excitatory and inhibitory effects of FUS with varying parameters in the 220–250 kHz pulse frequency range, with unknown mechanisms of actions on neurons and circuits [44–46]. Using BOLD fMRI signal as a readout, we have previously shown that blocks of 250 kHz FUS pulses with 935 kPa amplitude not only excited the neurons at the target, but also activated, likely via propagating spiking activity, interconnected neurons in remote regions within the same functional network (the touch network in our case) and beyond in the primate brain [23]. Others have reported similar observations in the visual and somatosensory system of humans and non-human primates [42,47–51]. Theoretical modeling of the biological effects predicts that FUS can excite or inhibit neural activity [52]. A low duty cycle, FUS intensity, or both can lead to inhibitory effects. Our own calcium imaging study of mouse sensorimotor cortex brain slices found that FUS pulse with similar frequency could activate pyramidal neurons [53].

The application of such FUS pulses to rats [54] and rabbits [55] resulted in a reduction of evoked potentials [56]. FUS with parameters in a similar range also induced suppression in humans [57]. In the current study we explored the inhibitory effects of FUS on neuronal activity in the brain using MRI guidance and BOLD fMRI monitoring. Here we delivered blocks of FUS with 425 kPa amplitude at a targeted area 3a/3b concurrently with the presentation of tactile stimulation of digits.

We observed both activation and suppression of medium amplitude FUS on neurons in stimulated target area 3a/3b. Using the tactile stimulation evoked fMRI neural activation as a reference, we discovered that medium amplitude FUS led to suppressed tactile stimulus-evoked neural responses but also directly activated neurons within the target at resting state when it was applied alone. The observation of significantly reduced tactile stimulation evoked BOLD signal changes during the concurrent delivery of FUS at the target area 3a/3b during peripheral tactile stimulation, which activates areas 3a/3b neurons, support the Inhibitory effects of FUS. Importantly, reductions of BOLD signals were also detected in

five downstream interconnected off-target brain regions (areas 1/2, S2, MCC, VPL, and insula). Since area 3a/3b is the first cortical relay station for innocuous tactile inputs, these BOLD signal reductions could be direct consequences of reduced driven activity from area 3a/3b by med-FUS. These state-dependent (activation versus at rest) dual modulatory effects at the target led us to speculate that activation (stimulation) and suppression effects of med-amplitude FUS could be mediated through stimulating different populations of neurons (i.e., excitatory pyramidal neurons and small inhibitory interneurons). The physiological state (active or rest) of neurons in the stimulated region and its circuit and how these neurons interact with each other during modulation could also influence the net outcome. For example, in areas 3a/3b, pyramidal cells in cortical layer IV receive predominantly cutaneous tactile and proprioceptive inputs from the thalamic VPL nucleus, they process the information via local microcircuits, and then send outputs to higher order areas 1/2 and S2 by pyramidal cells at deeper layer V. Large pyramidal cells are also surrounded by local small interneurons that are predominantly inhibitory. During local processing and integration, small interneurons interact with pyramidal neurons, modulate their activity, and sometimes gate their output information [58]. Direct activation of pyramidal neurons by FUS could subsequently excite interconnected neurons in different off-target regions via propagated spiking activity. Together, the dual modulation capacity of med-FUS is highly desirable as a brain stimulation and neuromodulation tool. The observed state dependence of the FUS modulatory effect is in line with those observed in TMS applications [25,26]. This state dependence is of high clinical significance since it likely will influence the efficacy of using FUS modulation as a therapeutic intervention. The net FUS modulatory effects will not only determined by the FUS parameters but also by the activation state of the brain, which could be drastically different in patients.

A second finding is that direct med-FUS stimulation of the area 3a/3b tactile region activated remote zones that do not spatially overlap with tactile responsive zones, suggesting that those off-target areas being modulated are not part of the classical tactile circuit that are driven by cutaneous inputs. Region based time course analysis support this observation (Fig. 6). The distinct medium amplitude FUS-induced fMRI network activation pattern cannot be explained by local off-target effects because (1) the ARFI maps confirmed that the FUS precisely targeted the tactile-evoked fMRI activation focus and (2) concurrent delivery of med-FUS suppressed tactile responses. This observation raises another possibility that med-amplitude FUS may preferentially activate subsets of different functional neurons such as the fast-adapting neurons over slow-adapting neurons that are driven by 8 Hz vibrotactile neurons in area 3b or proprioceptive neurons in area 3a [27,59]. Observations of quite distinct response features to med-FUS versus med-FUS + tactile stimulation in each of the other five brain regions of areas 1/2, S2, insula, MCC, and thalamus (Figs. 4 and 5) further support this hypothesis. Even though these brain regions have direct anatomical connections to area 3a/3b [60,61], it is unclear what drives the response differences in the off-target regions. It is possible that the connection strength and/or the number of synaptic connections play a role in leading to different down-stream neural modulations. Nevertheless, these findings are significant because for the first time they demonstrate that FUS may act on different populations of neurons. FUS has potential to probe direct causal functional

relationships between brain regions and to dissect brain circuits with some level of neuron-selectivity.

Med-FUS alone induced strong BOLD signal changes at the targets and off-targets regions, in magnitudes that are comparable to those of tactile stimulation in some regions (Fig. 5). Med-FUS induced BOLD signal changes in areas 3a/3b, MCC, and VPL exhibited a two-phase feature: an apparent signal drop at the beginning of the med-FUS stimulation followed by BOLD signal increases. The overall shape of the BOLD signal changes modulated by long med-FUS blocks is very similar to the typical hemodynamic signal changes evoked by natural tactile stimulation, which are believed to be related to increases in spiking activities and local field potentials in areas 3b and 1 of S1, as well as S2, within the monkey somatosensory system [34,62]. We interpret the responses of the off-target regions as neural-based and activated via inter-regional connections. Very weak MRI signals in adjacent white matter and in a resting state support our conclusion that FUS-induced effects are region- and circuit-selective, rather than global, non-neural effects in the brain.

Our data support that FUS's modulatory effects on fMRI signals are neural based, not a byproduct of non-neural vascular phenomena. FMRI signal is an indirect readout of neural activity and can be influenced by neurovascular coupling, therefore, there is a possibility that med-FUS induced fMRI signal change can be attributed to FUS-induced vascular changes at the target. If this was the case, then there would be no fMRI signal differences between med-FUS and med-FUS + tactile conditions in off-target regions because vasculature-mediated fMRI signal changes would not propagate along the tactile pathway to distant brain regions. If FUS modulation has neuronal origins, we would expect to detect differential downstream effects in different brain regions that are known to have connections to the FUS target of area 3a/3b. Indeed, this is what we observed. We detected significant differences between target and different off-target ROIs and between tactile alone and FUS conditions with and without tactile stimulation (Fig. 7). These differences can only be explained by FUS-induced neural activity changes at the target and down-stream neural activity in distant off-target regions.

It is worth noting that though the off-target effects of med-FUS on spatially remote regions are likely mediated by neuronal spiking activities, the suppressive effects of FUS on fMRI BOLD signals at the target could potentially be mediated through changes in the degree of neurovascular coupling. When concurrent FUS pulses interact with activated tactile neurons, it is conceivable that increased energy demands could reduce the tissue oxygenation level and thereby reduce BOLD signals. The neurovascular coupling and energy consumption are likely different during tactile stimulation + FUS versus Tactile- or FUS-alone conditions. In our study, blocks of 30 s stimulation were used to maximize BOLD signals, and it is expected that BOLD signals saturate once maximal vasodilation has been achieved. Whether additional metabolic demands can then cause reduction in BOLD signals has not been demonstrated.

Finally, it is worth noting the impact of anesthesia on fMRI signals and the interaction between FUS and cortical neurons. Isoflurane anesthesia typically suppress the neural response to stimulation (tactile stimulation in our case) and suppress the high frequency

component of electrical signal at resting state. Our group specifically addressed these issues previously. In our previous studies comparing the intrinsic functional imaging signals in awake versus isoflurane anesthetized monkeys, we found that light anesthesia indeed improves signal noise ratio that enhances the detection of functional signal changes in the areas 3b and 1 in monkeys [63]. When we examined the effects of isoflurane on fMRI signal at resting state, we found that low levels of isoflurane (~1%) that were used in the current study have a significantly weaker influence in somatosensory areas [64]. Importantly, under the same level of isoflurane, we were able to record robust local field potential and spiking activity of classic mechanoreceptive neurons in early somatosensory cortices. Thus, together, we think the isoflurane may help the detection of FUS induced fMRI signal changes by improving the signal-to-noise ratio in our case, because under anesthesia, the physiological noise associated with heart rate and respiration are drastically reduced. How isoflurane anesthesia influences the neuromodulation effects of FUS on higher order brain regions such as MCC or ACC remains to be determined.

The current study provided the first line of evidence supporting FUS state-dependent dual excitatory and inhibitory effects on target neurons and the ability to evaluate causal effects between interconnected neurons in a neuron-selective manner. We examined the theoretical concurrent excitatory and inhibitory effects at the whole brain level. We showed that medium amplitude and low-duty cycle FUS pulses activated concurrently two types of neurons, resulting in differential off-target responses depending on the specific connections between the target and off-target brain regions.

Supplementary Material

Refer to Web version on PubMed Central for supplementary material.

Acknowledgements

This work was funded by National Institutes of Health grants R01MH111877, R24MH109105, 1S10OD012297-01A1, 5T32EB014841, and 1F31EB026928, and the Focused Ultrasound Foundation. We would also like to acknowledge expert assistance from Chaohui Tang and Fuxue Xin for animal handling support, Tom Manuel for assistance with computer-aided design, and Jamie Reed for language editing of the manuscript.

Abbreviations

FUS	transcranial focused ultrasound
fMRI	functional magnetic resonance imaging
BOLD	blood-oxygen-level-dependent imaging
TES	transcranial electrical stimulation
ICS	intracranial electrical stimulation
DBS	deep brain stimulation
TMS	transcranial magnetic stimulation
MR-ARFI	magnetic resonance-acoustic radiation force imaging

HRF	hemodynamic response function
ROI	regions of interest
VPL	ventroposterior lateral
S2	secondary somatosensory cortex
Ins	insular cortex
MCC	Midcingulate cortex

References

[1]. Assaf M, Jagannathan K, Calhoun VD, Miller L, Stevens MC, Sahl R, et al. Abnormal functional connectivity of default mode sub-networks in autism spectrum disorder patients. Neuroimage 2010;53(1):247–56. [PubMed: 20621638]

[2]. Bai F, Watson DR, Yu H, Shi Y, Yuan Y, Zhang Z. Abnormal resting-state functional connectivity of posterior cingulate cortex in amnestic type mild cognitive impairment. Brain Res 2009;1302:167–74. [PubMed: 19765560]

[3]. Camchong J, Macdonald AW 3rd, Bell C, Mueller BA, Lim KO. Altered functional and anatomical connectivity in schizophrenia. Schizophr Bull 2011;37(3):640–50. [PubMed: 19920062]

[4]. Mayberg HS, Lozano AM, Voon V, McNeely HE, Seminowicz D, Hamani C, et al. Deep brain stimulation for treatment-resistant depression. Neuron 2005;45(5):651–60. [PubMed: 15748841]

[5]. Cauda F, Micon BM, Sacco K, Duca S, D'Agata F, Geminiani G, et al. Disrupted intrinsic functional connectivity in the vegetative state. J Neurol Neurosurg Psychiatry 2009;80(4):429–31. [PubMed: 19289479]

[6]. Fingelkurts AA, Kahkonen S. Functional connectivity in the brain–is it an elusive concept? Neurosci Biobehav Rev 2005;28(8):827–36. [PubMed: 15642624]

[7]. Fox MD, Halko MA, Eldaief MC, Pascual-Leone A. Measuring and manipulating brain connectivity with resting state functional connectivity magnetic resonance imaging (fcMRI) and transcranial magnetic stimulation (TMS). Neuroimage 2012;62(4):2232–43. [PubMed: 22465297]

[8]. Beric A. Transcranial electrical and magnetic stimulation. Adv Neurol 1993;63: 29–42. [PubMed: 8279314]

[9]. Mills KR, Murray NM, Hess CW. Magnetic and electrical transcranial brain stimulation: physiological mechanisms and clinical applications. Neurosurgery 1987;20(1):164–8. [PubMed: 3543723]

[10]. Turi Z, Paulus W, Antal A. Functional neuroimaging and transcranial electrical stimulation. Clin EEG Neurosci 2012;43(3):200–8. [PubMed: 22956648]

[11]. Saiote C, Turi Z, Paulus W, Antal A. Combining functional magnetic resonance imaging with transcranial electrical stimulation. Front Hum Neurosci 2013;7: 435. [PubMed: 23935578]

[12]. Ure JA, Olivier A, Quesney LF, Bravo M, Perassolo M. Temporolimbic activation by intracranial electrical stimulation. Can J Neurol Sci 2009;36(5):593–8. [PubMed: 19831128]

[13]. Stehberg J, Levy D, Zangen A. Impairment of aversive memory reconsolidation by localized intracranial electrical stimulation. Eur J Neurosci 2009;29(5): 964–9. [PubMed: 19200060]

[14]. Martin JC, Dougan JD, Wu Q, Stanisz LA, Martyn S, Rokosik S, et al. Locomotion induced by non-contingent intracranial electrical stimulation: Dopamine dependence and general characteristics. Behav Process 2004;67(2):131–46.

[15]. Signorelli F, Guyotat J, Mottolese C, Schneider F, D'Acunzi G, Isnard J. Intraoperative electrical stimulation mapping as an aid for surgery of intracranial lesions involving motor areas in children. Childs Nerv Syst 2004;20(6):420–6. [PubMed: 15133701]

[16]. Anderson RJ, Frye MA, Abulseoud OA, Lee KH, McGillivray JA, Berk M, et al. Deep brain stimulation for treatment-resistant depression: efficacy, safety and mechanisms of action. Neurosci Biobehav Rev 2012;36(8):1920–33. [PubMed: 22721950]

[17]. Awan NR, Lozano A, Hamani C. Deep brain stimulation: current and future perspectives. Neurosurg Focus 2009;27(1):E2.

[18]. Collins KL, Lehmann EM, Patil PG. Deep brain stimulation for movement disorders. Neurobiol Dis 2010;38(3):338–45. [PubMed: 19969083]

[19]. Nahas Z, Lomarev M, Roberts DR, Shastri A, Lorberbaum JP, Teneback C, et al. Unilateral left prefrontal transcranial magnetic stimulation (TMS) produces intensity-dependent bilateral effects as measured by interleaved BOLD fMRI. Biol Psychiatr 2001;50(9):712–20.

[20]. Berenyi A, Belluscio M, Mao D, Buzsaki G. Closed-loop control of epilepsy by transcranial electrical stimulation. Science 2012;337(6095):735–7. [PubMed: 22879515]

[21]. Haraldsson HM, Ferrarelli F, Kalin NH, Tononi G. Transcranial Magnetic Stimulation in the investigation and treatment of schizophrenia: a review. Schizophr Res 2004;71(1):1–16. [PubMed: 15374567]

[22]. Pollak TA, Nicholson TR, Edwards MJ, David AS. A systematic review of transcranial magnetic stimulation in the treatment of functional (conversion) neurological symptoms. J Neurol Neurosurg Psychiatry 2014;85(2):191–7. [PubMed: 23303960]

[23]. Yang PF, Phipps MA, Newton AT, Chaplin V, Gore JC, Caskey CF, et al. Neuromodulation of sensory networks in monkey brain by focused ultrasound with MRI guidance and detection. Sci Rep 2018;8(1):7993. [PubMed: 29789605]

[24]. Naor O, Krupa S, Shoham S. Ultrasonic neuromodulation. J Neural Eng 2016;13(3):031003. [PubMed: 27153566]

[25]. Silvanto J, Pascual-Leone A. State-dependency of transcranial magnetic stimulation. Brain Topogr 2008;21(1):1–10. [PubMed: 18791818]

[26]. Silvanto J, Muggleton NG, Cowey A, Walsh V. Neural adaptation reveals state-dependent effects of transcranial magnetic stimulation. Eur J Neurosci 2007;25(6):1874–81. [PubMed: 17408427]

[27]. Kaas JH. Evolution of somatosensory and motor cortex in primates. Anat Rec A Discov Mol Cell Evol Biol 2004;281(1):1148–56. [PubMed: 15470673]

[28]. Kaas JH, Collins CE. The organization of somatosensory cortex in anthropoid primates. Adv Neurol 2003;93:57–67. [PubMed: 12894401]

[29]. Chen LM. Cortical representation of Pain and touch: evidence from combined functional neuroimaging and electrophysiology in non-human primates. Neurosci Bull 2018;34(1):165–77. [PubMed: 28466257]

[30]. Chen LM, Dillenburger BC, Wang F, Friedman RM, Avison MJ. High-resolution functional magnetic resonance imaging mapping of noxious heat and tactile activations along the central sulcus in New World monkeys. Pain 2011;152(3):522–32. [PubMed: 21177033]

[31]. Chen LM, Turner GH, Friedman RM, Zhang N, Gore JC, Roe AW, et al. High-resolution maps of real and illusory tactile activation in primary somatosensory cortex in individual monkeys with functional magnetic resonance imaging and optical imaging. J Neurosci 2007;27(34):9181–91. [PubMed: 17715354]

[32]. Chen LM, Yang PF, Wang F, Mishra A, Shi Z, Wu R, et al. Biophysical and neural basis of resting state functional connectivity: evidence from non-human primates. Magn Reson Imaging 2017;39:71–81. [PubMed: 28161319]

[33]. Wu R, Wang F, Yang PF, Chen LM. High-resolution functional MRI identified distinct global intrinsic functional networks of nociceptive posterior insula and S2 regions in squirrel monkey brain. Neuroimage 2017;155:147–58. [PubMed: 28461059]

[34]. Wu R, Yang PF, Chen LM. Correlated disruption of resting-state fMRI, LFP, and Spike connectivity between area 3b and S2 following spinal Cord Injury in monkeys. J Neurosci 2017;37(46):11192–203. [PubMed: 29038239]

[35]. Phipps MA, Jonathan SV, Yang PF, Chaplin V, Chen LM, Grissom WA, et al. Considerations for ultrasound exposure during transcranial MR acoustic radiation force imaging. Sci Rep 2019;9(1):16235. [PubMed: 31700021]

[36]. Chaplin V, Phipps MA, Jonathan SV, Grissom WA, Yang PF, Chen LM, et al. On the accuracy of optically tracked transducers for image-guided transcranial ultrasound. Int J Comput Assist Radiol Surg 2019;14(8):1317–27. [PubMed: 31069643]

[37]. Hertzberg Y, Volovick A, Zur Y, Medan Y, Vitek S, Navon G. Ultrasound focusing using magnetic resonance acoustic radiation force imaging: application to ultrasound transcranial therapy. Med Phys 2010;37(6):2934–42. [PubMed: 20632605]

[38]. Saleem KSL NK. A combined MRI and Histology atlas of the rhesus monkey brain in stereotaxic coordinates. 2nd edition with horizontal, coronal, and sagittal series.: elsevier/academic press. 2012.

[39]. Yang PF, Qi HX, Kaas JH, Chen LM. Parallel functional Reorganizations of somatosensory areas 3b and 1, and S2 following spinal Cord Injury in squirrel monkeys. J Neurosci 2014;34(28):9351–63. [PubMed: 25009268]

[40]. Stringer EA, Chen LM, Friedman RM, Gatenby C, Gore JC. Differentiation of somatosensory cortices by high-resolution fMRI at 7 T. Neuroimage 2011;54(2):1012–20. [PubMed: 20887793]

[41]. Sanchez-Panchuelo RM, Francis S, Bowtell R, Schluppeck D. Mapping human somatosensory cortex in individual subjects with 7T functional MRI. J Neurophysiol 2010;103(5):2544–56. [PubMed: 20164393]

[42]. Lee W, Kim H, Jung Y, Song I-U, Chung YA, Yoo S-S. Image-guided transcranial focused ultrasound stimulates human primary somatosensory cortex. Sci Rep 2015;5.

[43]. Ye PP, Brown JR, Pauly KB. Frequency dependence of ultrasound neurostimulation in the mouse brain. Ultrasound Med Biol 2016;42(7):1512–30. [PubMed: 27090861]

[44]. Deffieux T, Younan Y, Wattiez N, Tanter M, Pouget P, Aubry JF. Low-intensity focused ultrasound modulates monkey visuomotor behavior. Curr Biol 2013;23(23):2430–3. [PubMed: 24239121]

[45]. Wattiez N, Constans C, Deffieux T, Daye PM, Tanter M, Aubry JF, et al. Transcranial ultrasonic stimulation modulates single-neuron discharge in macaques performing an antisaccade task. Brain Stimul 2017;10(6):1024–31. [PubMed: 28789857]

[46]. Fomenko A, Neudorfer C, Dallapiazza RF, Kalia SK, Lozano AM. Low-intensity ultrasound neuromodulation: an overview of mechanisms and emerging human applications. Brain Stimul 2018;11(6):1209–17. [PubMed: 30166265]

[47]. Lee W, Kim HC, Jung Y, Chung YA, Song IU, Lee JH, et al. Transcranial focused ultrasound stimulation of human primary visual cortex. Sci Rep 2016;6: 34026. [PubMed: 27658372]

[48]. Folloni D, Verhagen L, Mars RB, Fouragnan E, Constans C, Aubry JF, et al. Manipulation of subcortical and deep cortical activity in the primate brain using transcranial focused ultrasound stimulation. Neuron 2019;101(6): 1109–11016 e5. [PubMed: 30765166]

[49]. Verhagen L, Gallea C, Folloni D, Constans C, Jensen DE, Ahnine H, et al. Offline impact of transcranial focused ultrasound on cortical activation in primates. Elife 2019;8.

[50]. Legon W, Sato TF, Opitz A, Mueller J, Barbour A, Williams A, et al. Transcranial focused ultrasound modulates the activity of primary somatosensory cortex in humans. Nat Neurosci 2014;17(2):322–9. [PubMed: 24413698]

[51]. Ai L, Bansal P, Mueller JK, Legon W. Effects of transcranial focused ultrasound on human primary motor cortex using 7T fMRI: a pilot study. BMC Neurosci 2018;19(1):56. [PubMed: 30217150]

[52]. Plaksin M, Kimmel E, Shoham S. Cell-type-selective effects of intramembrane cavitation as a unifying theoretical framework for ultrasonic neuromodulation. eNeuro 2016;3(3). ENEURO. 0136–15.

[53]. Manuel Thomas J, Kusunose Jiro, Xiaoyan Zhan, Xiaohui Lv, Ellison Kang, Aaron Yang, et al. Ultrasound neuromodulation depends on pulse repetition frequency and can modulate inhibitory effects of TTX. Sci Rep 2020;10(1): 15347. [PubMed: 32948791]

[54]. Kim H, Park MY, Lee SD, Lee W, Chiu A, Yoo SS. Suppression of EEG visual-evoked potentials in rats through neuromodulatory focused ultrasound. Neuroreport 2015;26(4):211–5. [PubMed: 25646585]

[55]. Yoo SS, Bystritsky A, Lee JH, Zhang Y, Fischer K, Min BK, et al. Focused ultrasound modulates region-specific brain activity. Neuroimage 2011;56(3): 1267–75. [PubMed: 21354315]

[56]. Dallapiazza RF, Timbie KF, Holmberg S, Gatesman J, Lopes MB, Price RJ, et al. Noninvasive neuromodulation and thalamic mapping with low-intensity focused ultrasound. J Neurosurg 2018;128(3):875–84. [PubMed: 28430035]

[57]. Legon W, Bansal P, Tyshynsky R, Ai L, Mueller JK. Transcranial focused ultrasound neuromodulation of the human primary motor cortex. Sci Rep 2018;8(1):10007. [PubMed: 29968768]

[58]. Chu J, Anderson SA. Development of cortical interneurons. Neuropsychopharmacology 2015;40(1):16–23. [PubMed: 25103177]

[59]. Xu Y, Wang X, Peck C, Goldberg ME. The time course of the tonic oculomotor proprioceptive signal in area 3a of somatosensory cortex. J Neurophysiol 2011;106(1):71–7. [PubMed: 21346201]

[60]. Morecraft RJ, Stilwell-Morecraft KS, Cipolloni PB, Ge J, McNeal DW, Pandya DN. Cytoarchitecture and cortical connections of the anterior cingulate and adjacent somatomotor fields in the rhesus monkey. Brain Res Bull 2012;87(4e5):457–97. [PubMed: 22240273]

[61]. Morecraft RJ, Stilwell-Morecraft KS, Ge J, Cipolloni PB, Pandya DN. Cytoarchitecture and cortical connections of the anterior insula and adjacent frontal motor fields in the rhesus monkey. Brain Res Bull 2015;119(Pt A):52–72. [PubMed: 26496798]

[62]. Wang Z, Chen LM, Negyessy L, Friedman RM, Mishra A, Gore JC, et al. The relationship of anatomical and functional connectivity to resting-state connectivity in primate somatosensory cortex. Neuron 2013;78(6):1116–26. [PubMed: 23791200]

[63]. Chen LM, Friedman RM, Roe AW. Optical imaging of digit topography in individual awake and anesthetized squirrel monkeys. Exp Brain Res 2009;196(3):393–401. [PubMed: 19484466]

[64]. Wu TL, Mishra A, Wang F, Yang PF, Gore JC, Chen LM. Effects of isoflurane anesthesia on resting-state fMRI signals and functional connectivity within primary somatosensory cortex of monkeys. Brain Behav 2016;6(12):e00591. [PubMed: 28032008]

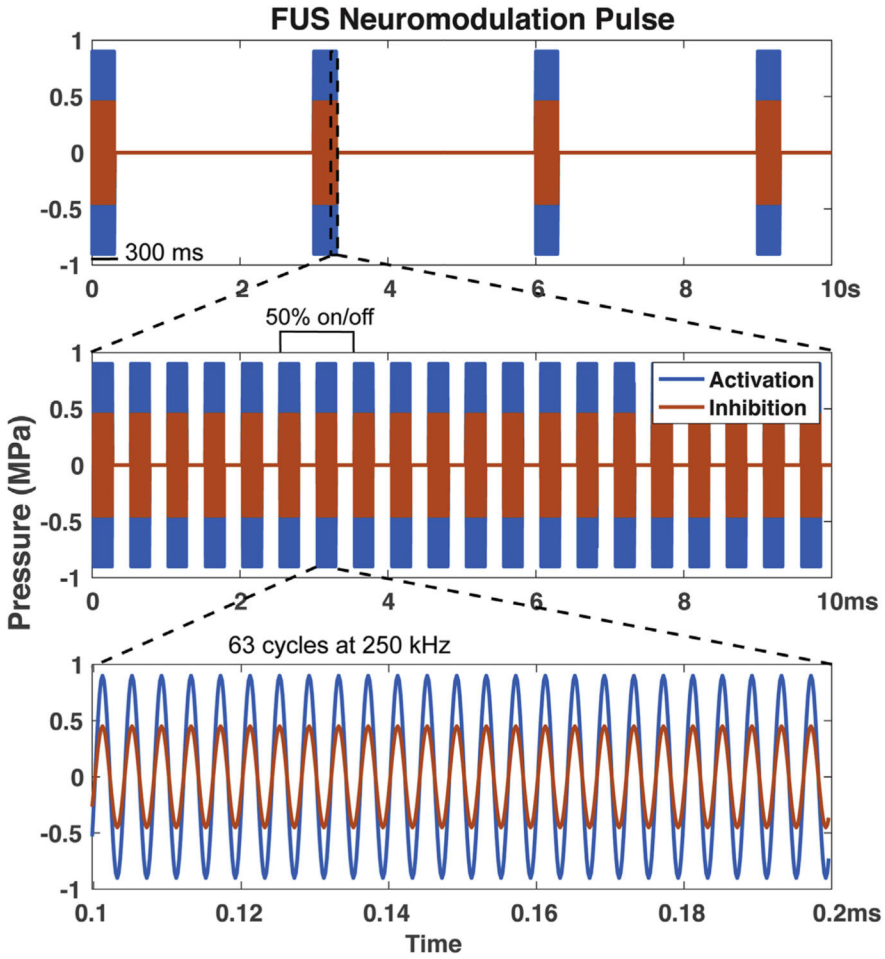

Fig. 1.

FUS pulse design. The blue curves represent FUS pulses with full pressure amplitude of 935 kPa used in our previous study [23], while the orange curves represent the lower (45%), medium amplitude FUS pulses at 425 kPa pressure used in the current study.

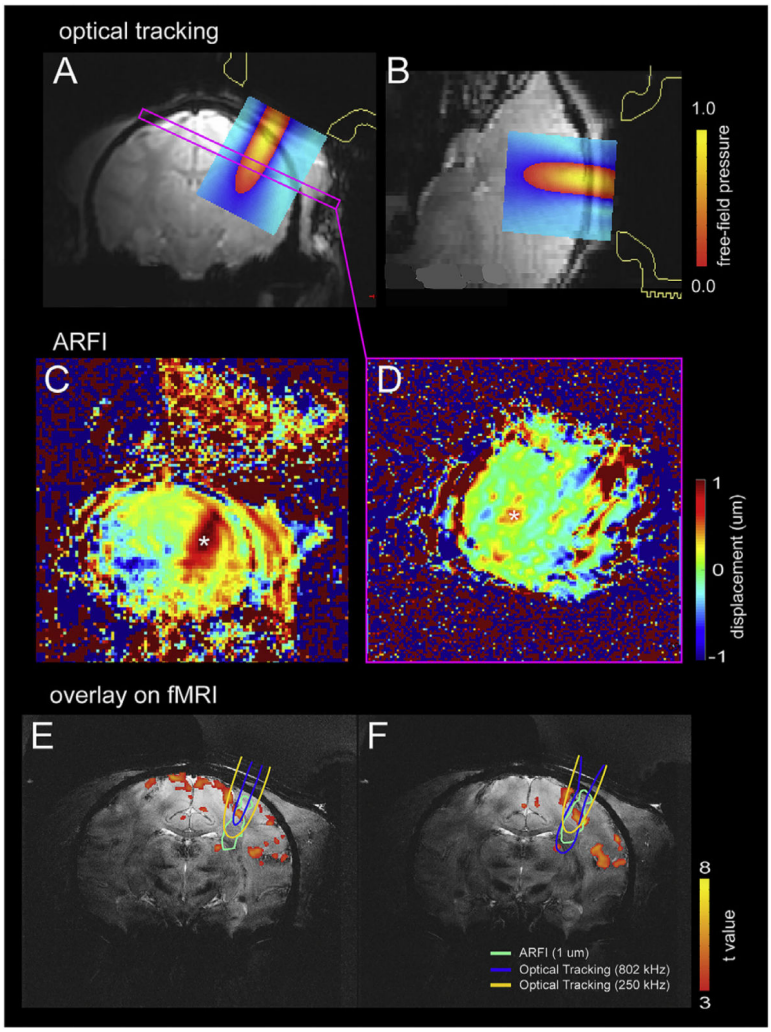

Fig. 2.

MRI guided FUS stimulation set up with optical tracking and real-time ARFI. (A–B) Views of the spatial relationships between the FUS transducer, optical tracking-based projection of the free-field beam, and the targeted brain region. Free-field FUS beam overlaid on MRI images in two imaging planes (A: coronal, B: sagittal). Color bars represent the scaled pressure range. (C–D) Intracranial ARFI maps on coronal (C) and oblique (D) images perpendicular to the FUS beam. Asterisks indicate the voxels that detected tissue displacement. Color scale: displacement in mm. (E–F) ARFI displacement contour maps overlaid on T2*-weighted structural coronal images (light green, thresholded at 1 mm), along with 802 and 250 kHz optical tracking-based free-field beam projections (blue and yellow outlines, respectively, thresholded at 50% of peak pressure), and with BOLD activation foci (thresholded at t = 3).

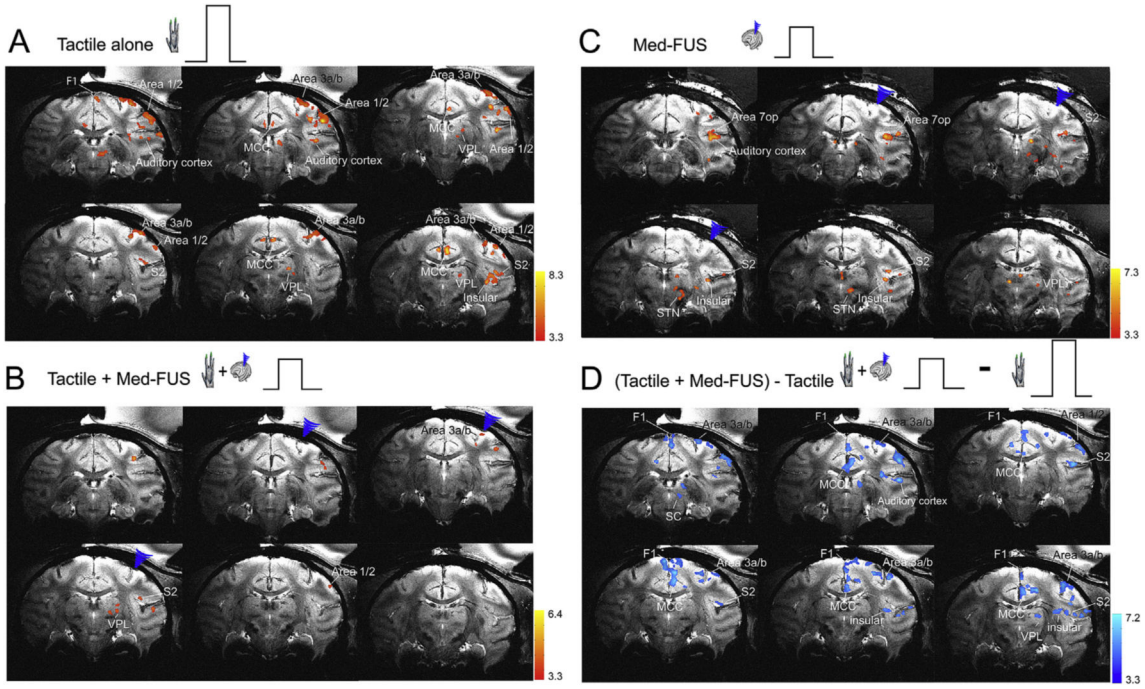

Fig. 3.

Concurrent sonication of areas 3a/3b with moderate amplitude FUS pulses suppresses tactile stimulus evoked fMRI BOLD activations in the brain of one macaque monkey (M1). (A) Multi-run coronal fMRI activation maps evoked by 8 Hz vibrotactile stimulation of distal finger pads of digits 2 & 3 of left hand. Activation maps with thresholds t > 3.3, $p = 0.001$, $q = 0.003$, FDR ($p < 0.05$) corrected. Nine coronal images are arranged from rostral to caudal direction (top left to bottom right). Blue arrowheads indicate the FUS transducer location. (B) Multi-run coronal fMRI activation maps evoked by concurrent delivery of tactile and medium amplitude FUS stimulation (Tactile + Med-FUS) of the areas 3a/3b region of right hemisphere. (C) Multi-run coronal fMRI activation maps evoked by medium amplitude FUS (Med-FUS) stimulation of the areas 3a/3b hand region. (D) fMRI subtraction maps of tactile stimulation plus medium amplitude FUS minus tactile stimulation ((Tactile + Med-FUS) - Tactile). WM: white matter. MCC: midcingulate cortex. Insula: insular cortex. 3a/b: areas 3a and 3b. 1–2: areas 1 & area 2. VPL: thalamic ventral-posterior-lateral nucleus. D: dorsal. V: ventral. L: left. R: right.

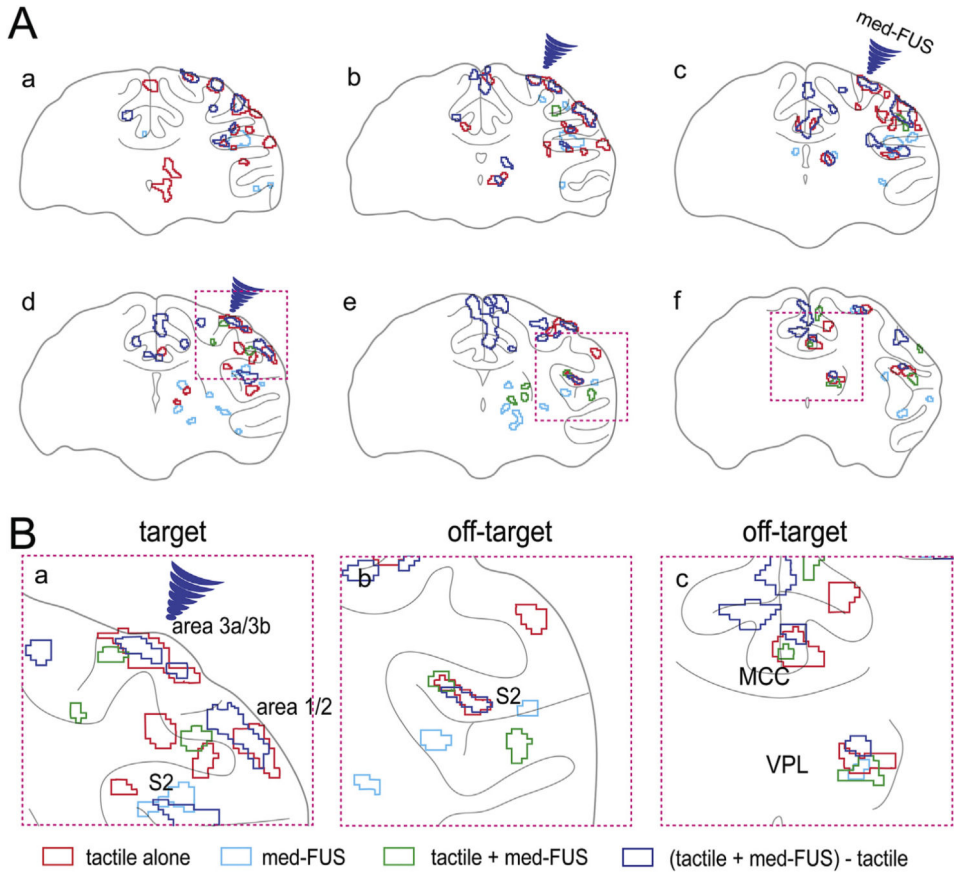

Fig. 4.

Spatial overlaps of fMRI activation foci in different experimental conditions. (A) The overlay of activation maps shown in Fig. 3 A–D. Blue arrowheads indicate the FUS beam focus. Three magenta dotted line boxes (d-f) indicate the field of views of zoomed-in illustration of the activation maps shown in B. (B) Zoomed-in views of composite four-condition BOLD activation maps show the spatial relationships of their corresponding evoked BOLD fMRI activation foci. Red outlines: tactile alone activation foci. Light blue outlines: activation to moderate intensity FUS. Green outlines: regions activated by simultaneous tactile + med-FUS stimulation. Blue outlines: regions exhibited greatest med-FUS induced BOLD signals difference.

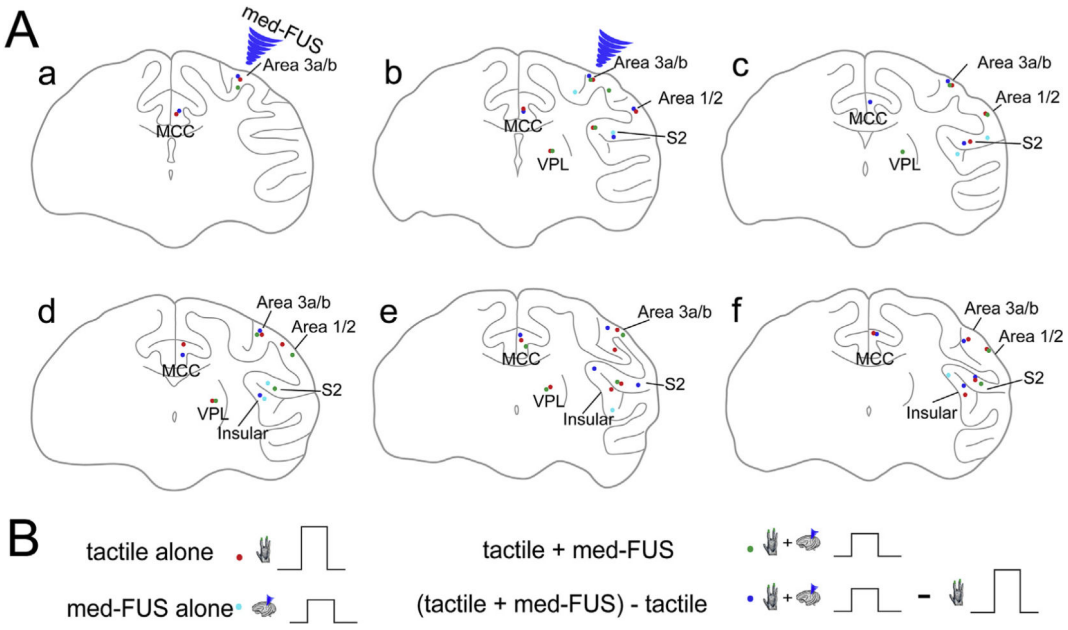

Fig. 5.

Spatial locations of BOLD fMRI activation foci. (A) Schematic map of the peak locations of activation loci identified in three conditions in subject one. (B) Experimental conditions. Blue arrowheads indicate the target locations of the FUS transducer.

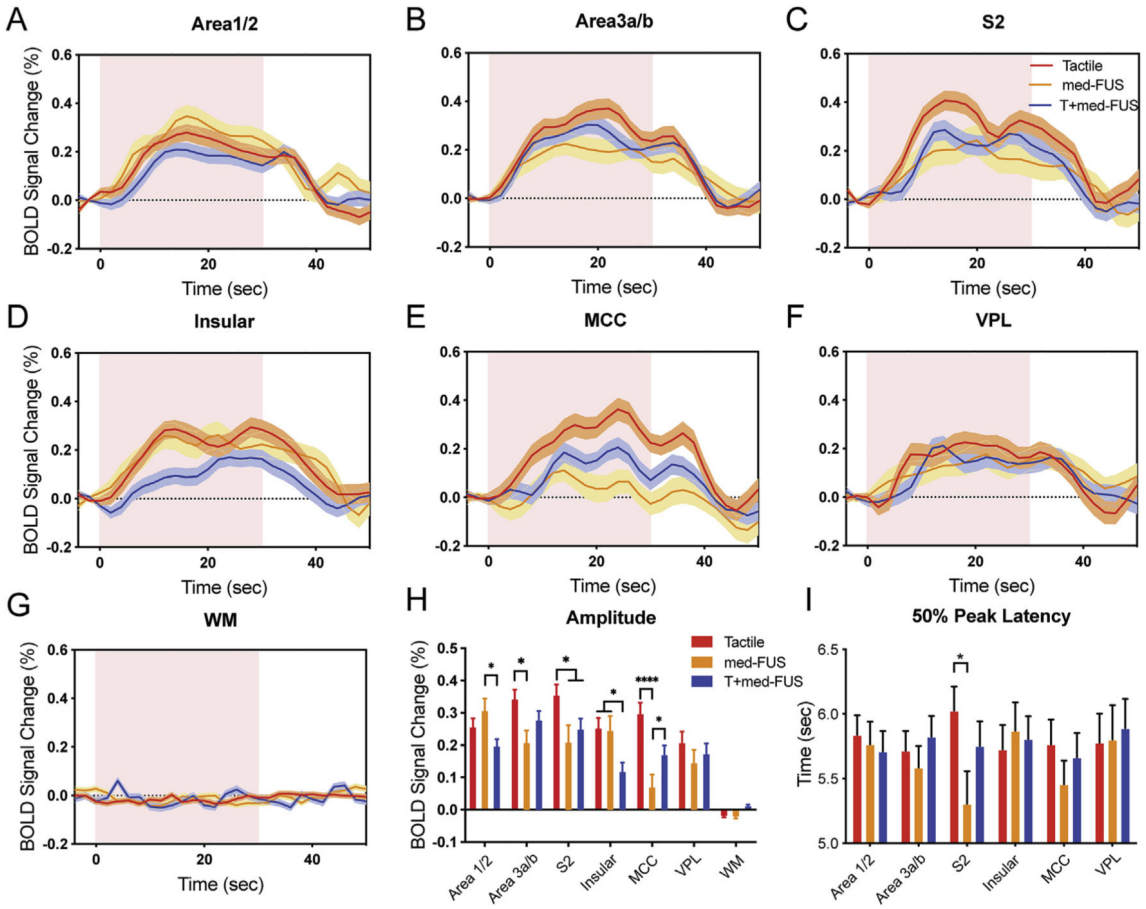

Fig. 6.

Comparison of time courses and peaks of BOLD signal changes in three stimulation conditions. (A-G) Time courses of % BOLD signal changes extracted from the all activated voxels (thresholded at t = 3.3) in six brain regions (area 1/2, area 3a/3b, S2, insular cortex, midcingulate cortex (MCC), ventroposterior lateral nucleus of thalamus (VPL)) and one control region in white matter (WM) during stimulation types: tactile alone (red), med-FUS alone (orange), and tactile + med-FUS (blue). Distribution of standard error indicated with a shade lighter than the mean lines. Pink background blocks indicate the 30-sec stimulation period. (H) Comparison of peak % BOLD signal changes in three stimulation conditions in each individual ROI. *$p < 0.05$, ****$p < 0.001$, one-way ANOVA followed by Tukey's test. (I) Times to reach 50% peak BOLD signal changes in each individual ROI. FMRI data from a total of 23 tactile, and 19 med-FUS + tactile, and 9 med-FUS alone runs from six imaging sessions in two animals were included in the group quantification.

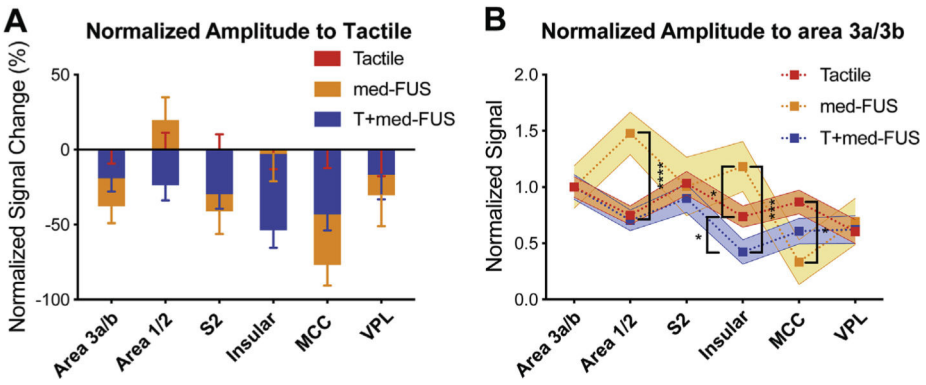

C

	3a/b	1/2	S2	Insular	MCC	VPL
Tactile	0	0	0	0	0	0
T+mFUS	-19.07	-23.83	-29.64	-53.64	-43.29	-16.64
mFUS	-37.76	19.64	-41.07	-2.771	-76.84	-30.41

D

	mFUS	T+mFUS	T
area 1/2	1.48	0.70	0.75
S2	1.00	0.90	1.04
Insular	1.18	0.42	0.74
MCC	0.33	0.61	0.87
VPL	0.69	0.62	0.60

Fig. 7.

Differential modulatory effects of med-FUS on different brain regions. (A, C) Comparison of effects of med-FUS and med-FUS + tactile stimulation with respect to tactile responses (normalized % BOLD signal changes to tactile condition) across regions (A). Positive values indicate stronger than tactile responses and negative values indicate weaker than tactile responses. Table C shows the mean % BOLD signal changes for each condition in each area (C). (B, D) Comparison of modulatory effects of med-FUS + tactile and med-FUS alone to the tactile responses of off-target regions respect to the target of area 3a/3b. Shaded regions surrounding the dotted lines indicate the range of standard error at each ROI. *$p < 0.05$, **$p < 0.01$, ***$p < 0.005$, ****$p < 0.001$, unpaired t-test. Table D shows the mean % BOLD signal changes.

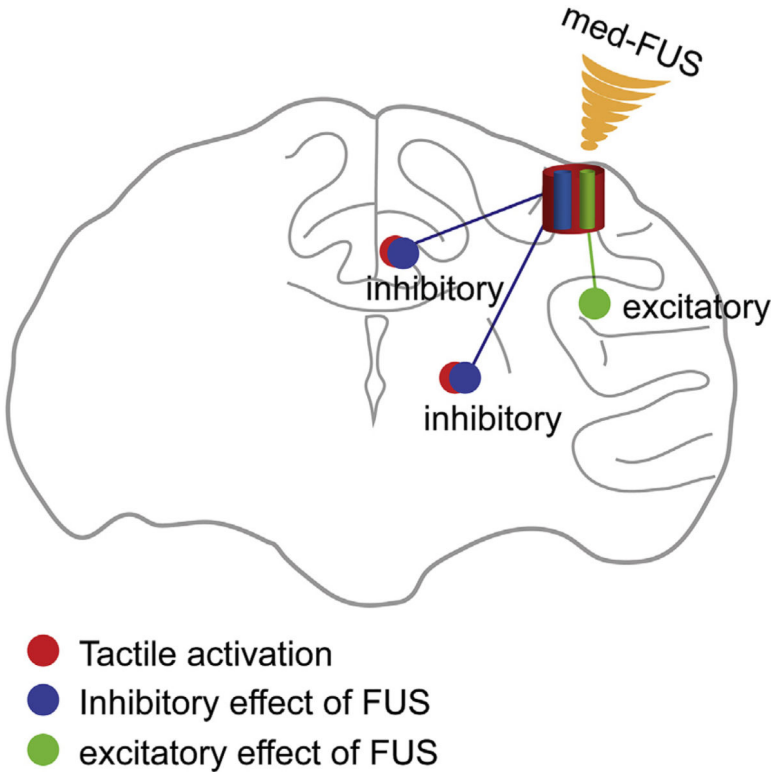

Fig. 8.

Schematic model of the FUS dual modulation of neuronal activity. Model shows that med-FUS induces dual modulatory effects on neurons: inhibition and excitation. The dual effects likely are mediated by excitation of two types or groups of neurons. For inhibitory effects, med-FUS may activate inhibitory interneurons that suppress peripheral stimulus driven tactile neuron activity. For excitation effects, med-FUS may activate pyramidal neurons that can transmit their activity to downstream interconnected neurons.